

## Mutual Coupling Reduction between Slotted-T MIMO Elements for UWB Applications

Kudumu V. Prasad<sup>1, \*</sup> and Makkapati V. S. Prasad<sup>2</sup>

**Abstract**—In the present scenario, multiple-input-multiple-output (MIMO) elements provide the capacity to generate more than one radiation pattern with different polarizations, which show a prodigious role in the modern telecommunication sector. A new two-element MIMO antenna with minimization in mutual coupling is presented in this paper. The proposed design reduces mutual coupling between antenna elements. The strip-line mechanism is used as a feed and is simulated using HFSS v 15. MIMO element design is done with four T-shaped slots in all directions of the patch, further enhancing the cross-correlation. MIMO antenna consists of two radiators on a  $50 \times 25 \text{ mm}^2$  FR-4 substrate. A T-shape ground stub, along with a slot, reduces mutual coupling (MC) and Impedance Bandwidth (IBW) of the proposed design. The design provides multi-band characteristics in the entire UWB range with practical applications like WiMAX (3.5 GHz), WLAN (5.9 GHz), X-band SATCOM applications (7.9 GHz) and Radar, Mobile phones, and commercial WLAN (9.3 GHz). The spacing between elements is in the order of  $0.215\lambda_0$ . MC reduction of 20 dB is achieved at every resonant frequency.

### 1. INTRODUCTION

MIMO is one of the dynamic research areas that provide wireless system efficiency, increase channel capacity, thus providing this technology as a key to the fifth generation (5G) networks, 4G, RFID, Digital Home, and WLAN. MC between elements in a MIMO antenna is a metric while the MIMO antenna performance is examined. When several antennas are nearby, they suffer from severe MC, which leads to the loss of bandwidth, lower antenna efficiency, decreased SINR, and degraded performance of diversity gain. MC's effect occurs between closely spaced antennas due to the surface current flow from the ports excited and surface waves. For portable devices with minimal space, mounting multiple low MC elements is a challenge for the designers [1]. There are different methods to improve isolation such as Electromagnetic Band Gap (EBG) structure [1, 16], shorting pins [2], metalized via wall [4], inserting single split-ring resonator (SRR) in-ground plane [7, 14], parasitic branches [7], a fractal EBG structure [8], defected ground structures (DGSs) [10–15], single lattice mushroom-like EBG [16, 19], a slot structure perpendicular to the current on the surface of patches on a common ground plane [17], and metamaterials [20].

A compact and wide-band MIMO element antenna for WLAN and WiMAX applications is studied and analyzed to integrate an EBG to reduce the MC between the ports. The frequency operating range is 2.01 to 3.92 GHz, which achieves a minimum MC of 29 dB [1]. In [2], isolation enhancement is done with the shorting pins. Six metallic pins via loading near the adjacent edges improve the MC reduction with different antenna polarizations. A minimum of  $0.012\lambda_0$  separation is used between two element edges. A square patch is modified so that, on the square radiator top, an L-shaped slot of inverted type is introduced. Three slots on the right and left sides of the square radiator and an ohm symbol at the

---

*Received 11 September 2020, Accepted 7 December 2020, Scheduled 17 December 2020*

\* Corresponding author: Kudumu Vara Prasad (kvprasad.vrsec@gmail.com).

<sup>1</sup> Research Scholar, ECE, ANU College of Engineering and Technology, Guntur, India. <sup>2</sup> R V R & J C College of Engineering, India.

center are proposed. This antenna achieves multi-band characteristics at 2.2 GHz, 4.1 GHz, 5.5 GHz, 5.9 GHz, and 9.1 GHz [3]. A compact structure with a low profile are introduced in [4] for reducing MC. In this, inverted H-shaped metal walls are used to reduce EM spatial coupling, and a folded T-branch is implemented to reduce EM surface waves. The design in [4] operates between 2.44 GHz and 3 GHz. A MIMO design for UWB applications with high isolation is proposed in [5].

The size of  $30.1 \times 20.5 \text{ mm}^2$  is used for the two monopole elements. This design proposes a protruded ground, and the feed-line bending is used as a technique. High isolation with low ECC for a MIMO design is proposed in [6]. A separation of  $0.13\lambda_0$  is used. Experimental results achieve isolation improvement by 22 dB. In [7], a dual-band MIMO antenna operating at X, Ku bands is designed with a parasitic element structure on an FR-4 substrate excited by orthogonal strip-line feeding.

Additionally, a single CSRR is used to improve performance characteristics. The proposed MIMO antenna achieves  $|S_{12}| < -26 \text{ dB}$  suitable for X and Ku bands. A compact UWB-MIMO antenna of fractal type is proposed using the iterated function system (IFS) [8]. A new technique termed self-similar fractal is implemented to provide wide-band performance with miniaturization. A T-stub with a slot improves the isolation of the proposed MIMO system. The proposed structure has  $24 \times 32 \text{ mm}^2$  dimensions operating from 3.1 to 12.5 GHz UWB with the isolation about 16 dB. A detailed investigation on reducing the MC in MIMO antennas using various mechanisms and structures is projected with examples [9].

An FDTD method, along with DGS, is used to reduce MC of a two-element array. The comparison of DGS structure with other techniques to analyze MC between two elements is done. In a MIMO antenna with four ports, isolation is improved by proposing DGS and is improved by 7 dB. The proposed structure includes a patch with a square ring DGS etched in the ground. A very compact UWB-MIMO antenna, consisting of two slot elements, is proposed with  $22 \times 26 \text{ mm}^2$ . A T-slot, ground-etched, is used to reduce MC and improves the impedance matching. An antenna design for reducing MC for WLAN application is proposed and consists of two radiating elements, six metal strips, ground, and a substrate. About  $-42 \text{ dB}$  MC at 5.8 GHz is obtained. A novel EBG with a metal strip is used to enhance MIMO isolation for the WLAN application. A metal line strip is used in between the elements for reducing the MC at 5.8 GHz. To eliminate scan blindness in a phased array, a U-shaped DGS is used. A U-shaped DGS provides better MC reduction by suppressing surface wave propagation. A U-shaped DGS along with patch array is studied with different distances, and the results show that the MC suppression is increased with the reduction in element distance [10–15].

In [16], when the distance between the array elements is minimal, a strong MC appears. Periodic structures like EBG are used to minimize the antenna array's MC by reducing the substrate-based surface waves at the operating frequency. The number of EBGs used is  $13 \times 2$  structures, and the MC is reduced to  $-59.36 \text{ dB}$  at 5.8 GHz. In [17], a compact triple band-notched MIMO antenna for UWB communication is proposed and designed with quarter-wavelength slots. These slots are placed between two radiators, which provide notch bands for the frequencies 3.3–4.2 GHz, 5–6 GHz, and 7.2–8.6 GHz. To reduce MC between patch elements, an I-shaped stub is used. In [18], a fractal regular slots monopole for UWB is proposed.

In [19], an approach to suppress the surface waves between two H-shaped MIMO patches is proposed. This proposed antenna uses an EBG as an isolator to minimize MC between the ports. In [20], to reduce MC, a slot antenna array using an electric metamaterial is designed. This method consists of an array of CSRRs between the two slots for reducing the MC propagation. Both complementary fishnet structures and CSRRs are used for better isolation. With both the structures and gap between elements being 3.4 mm,  $S_{12}$  achieves  $-14 \text{ dB}$  isolation improvement at 2 GHz.

In [21], a band-notched MIMO antenna with a size of  $22 \times 36 \text{ mm}^2$  for UWB applications is proposed. To reduce MC, the design utilizes two monopole elements, a slot cut on the T-stub, a T-stub, and two strips on the ground to generate notch frequency. Frequency 5.15–5.85 GHz is the notch band, and the antenna operates from 3.1 to 11 GHz.  $\text{MC} < -15 \text{ dB}$ . A fractal monopole of hybrid planar type is presented for MIMO antenna implementation. This structure is the grouping of the Koch curve fractals and the Minkowski island curve. The separation is  $0.16\lambda_0$ . A T-shape strip to improve the impedance matching is introduced, and the slot is carved on the ground topside to enhance isolation between the elements [22].

In [23], a novel bandpass filter of hairpin type with a modified Minkowski fractal geometry is

proposed. The filters with the fractal shape can significantly suppress the second harmonic of the filter design. In [24], a new all-metallic phase-correcting structure (AMPCS) is introduced for the usage of Electromagnetic Bandgap Resonator Antennas (ERAs) to reduce the fabrication cost, and the AMPCS is fabricated with laser technology and tested for an ERA application to verify its performance. In [25], a wide-band high-gain Resonant Cavity Antenna (RCA) with low-cost Partially Reflecting Surface (PRS) is proposed, and it requires a single commercial dielectric slab. A negative transverse-reflection magnitude gradient and a progressive reflection phase gradient are exhibited at 11.4 GHz frequency by the nonuniform double-sided printed dielectric, which is a characteristic of PRS. The directivity is 16.2 dBi at 11.4 GHz, and the peak gain is 15.75 dBi. In [26], an EBG resonator antenna's performance is analyzed at 60 GHz, and this antenna resonator achieves a directivity of 15.5 dB. For this, a PRS composed of four rings with different permittivities is designed, which achieves a wide-band radiation pattern. In [27], a MOPSO (Multi-Objective Stochastic) algorithm is proposed for a phased array. To maximize diversity performance, Particle Swarm Optimization (PSO) algorithm is used for the sidelobe suppression at maximum scan angle and minimizes the voltages induced at the receiver frontend. Aperture efficiency and mismatching are the energy constraints that are considered as inputs to the PSO algorithm. For this, an array with 16 dipoles is used to minimize the sidelobe level with  $60^\circ$  scanning rate and elements with  $\lambda/2$  apart. In [28], for improving radiation patterns and directivity, an efficient PSO algorithm is developed to design a near-field time delay equalizer metasurface (TDEM) of ERAs. In [29], a design methodology based on Bayesian Regularization Back-Propagation (BRBP) algorithm is proposed to design the microstrip filters. In this, to enhance the filter's performance, a filter is composed of stepped impedance resonators, and multiple open stubs are designed with the Artificial Neural Network (ANN) technique at the operating frequency 2.087 GHz.

Various researches in the introduction have discussed various methods to reduce mutual coupling. The antenna design proposed in this article is a miniaturized and straightforward design with T-shaped stubs as one of the reduction techniques for mutual coupling compared to some of the antenna designs proposed in the literature survey in the introduction section, and a comparison table is presented in Section 5.

The article is organized in the following way. Antenna design with different parameter analysis is explained in Section 2. Section 3 presents the study of the proposed design. Section 4 presents the parametric analysis of the proposed design. Simulation results and measurement results are explained in Section 5. Finally, Section 6 presents the conclusion.

## 2. PROPOSED ANTENNA DESIGN

Figure 1 shows a strip-line fed MIMO antenna with four slots of three different sizes on all the antenna element's four sides. This MIMO antenna is simulated and fabricated on an FR-4 with size  $W_s \times L_s$ ,  $\epsilon_r = 4.4$ , and  $\tan \delta = 0.002$  using HFSS. A T-stub is positioned in between two T-shaped slotted MIMO elements, shown in Figure 1. This technique uses a square element with  $L_p \times W_p$ ; four equal slots of two different sizes are subtracted on all four sides with  $L_1, L_2, L_3$  lengths, and  $W_1, W_2,$  and  $W_3$  widths. This MIMO design is excited with a  $50 \Omega$  strip-line, and the distance between the two elements is 10.75 mm.

A seven-stage MIMO design is shown in Figure 2 to explain the antenna progress.

The mathematical expressions for the antenna evolution stages are:

$$\epsilon_{r_{eff}} = \left( \frac{\epsilon_r + 1}{2} \right) + \left( \left( \frac{\epsilon_r + 1}{2} \right) \left( 1 + \frac{12h}{w} \right)^{-\frac{1}{2}} \right) \quad (1)$$

The condition to suppress surface waves,

$$\frac{h}{\lambda_0} \leq \frac{0.3}{2\pi\sqrt{\epsilon_0}} \quad (2)$$

$$L_e = \frac{c}{2f_0\sqrt{\epsilon_{eff}}} \quad (3)$$

$$\text{Length of the patch, } L = L_e - 2\Delta L \quad (4)$$

$$\text{Length of the stub 1, } L_3 \simeq \lambda/4 \quad (5)$$

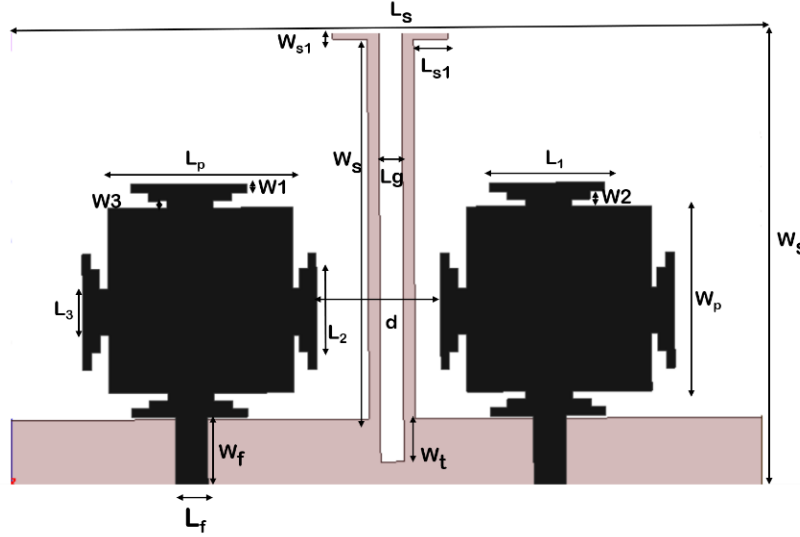


Figure 1. A proposed MIMO antenna structure.

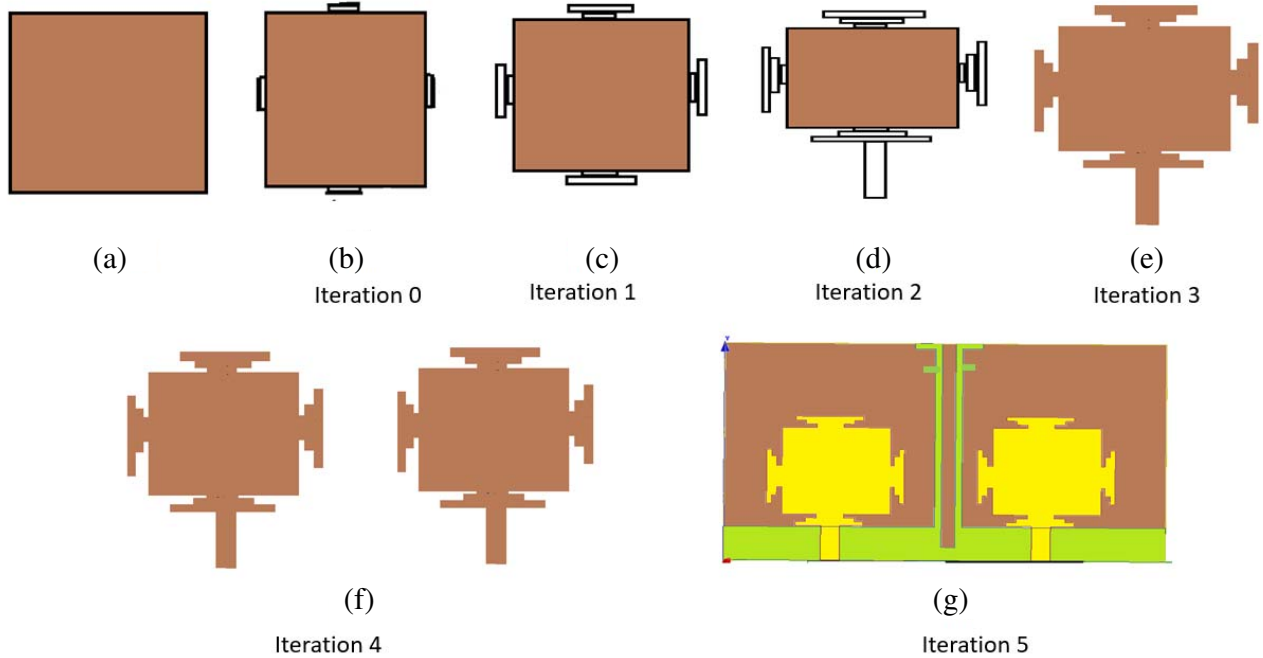


Figure 2. Proposed MIMO antenna evolution stages.

$$\text{Length of the stub 2, } L_2 \simeq L_3 + 2(\lambda/4) \tag{6}$$

$$\text{Length of the stub 3, } L_1 \simeq 2(L_3) + 2(\lambda/4) \tag{7}$$

The parameters optimized for the design are listed in Table 1. In this, a square MIMO element is used and operates in the UWB frequency range with specific applications at WiMAX (3.5 GHz), WLAN (5.9 GHz), X-band SATCOM (7.9 GHz) and Radar, Mobile phones, and commercial WLAN (9.3 GHz). Rectangular slots with three different lengths of the MIMO element are used to resonate at different frequencies.

The simulated  $S_{11}$  and  $S_{12}$  for the design proposed are shown in Figure 3. Similarly, the same procedure is applied to all four sides of the patch at different evolution stages. Finally, the MIMO

**Table 1.** Design parameters of the proposed MIMO design.

Parameter	$L_s$	$W_s$	$L_p$	$W_p$	$L_1$	$L_2$	$L_3$	$W_1$	$W_2$
Value (mm)	50	25	16	16	10	7.2	4	1	0.8
Parameter	$W_3$	$L_f$	$W_f$	$L_{s1}$	$W_{s1}$	$L_g$	$W_s$	$W_t$	$d$
Value (mm)	50	25	16	16	10	7.2	4	1	0.8

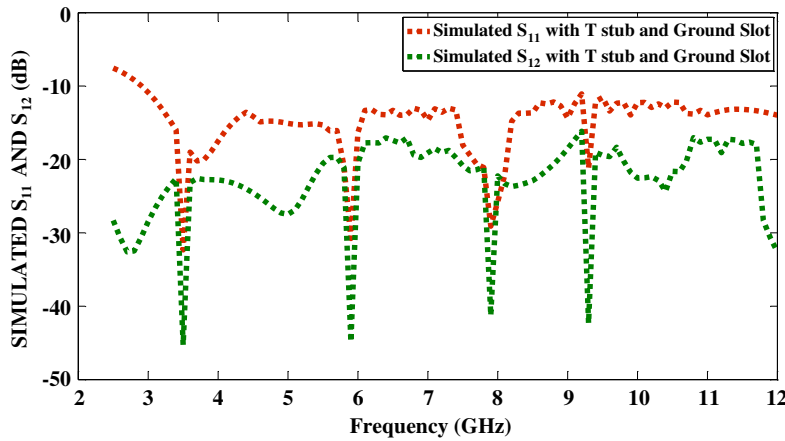


**Figure 3.**  $S_{11}$  and  $S_{12}$  of the proposed MIMO design.

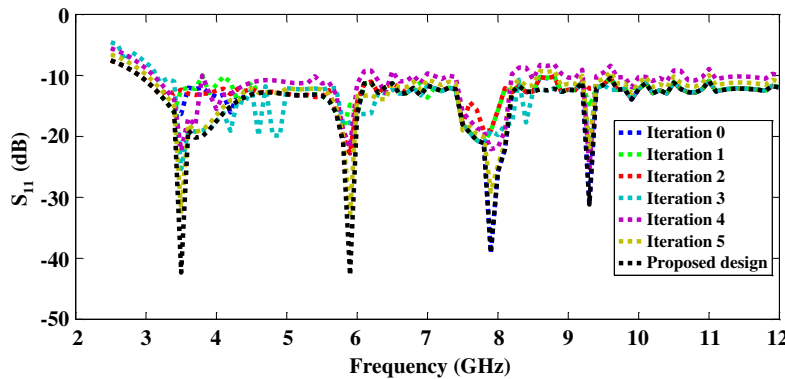


**Figure 4.**  $S_{11}$  for the different stages of the proposed MIMO.

antenna is represented in Figure 2(g) resonating from 2.77 GHz to 6.65 GHz with  $|S_{11}| < -10$  dB being identified. In the proposed design,  $|S_{12}| < -20$  dB is observed. Figure 4 shows  $S_{11}$  for different MIMO antenna stages, in which the antenna resonates from the square patch structure to the final design of the MIMO antenna, suitable for WiMAX and WLAN.

A T-stub is positioned between slot-cut MIMO elements for necessary impedance matching. To enhance MC, in the ground, a slot of a small portion is etched. Table 1 includes dimensions of the proposed MIMO antenna.

### 3. STUDY OF PROPOSED ANTENNA

#### 3.1. T-Shape Stub Effect

The concept of the T-shape stub used in the MIMO concept is proposed in [7, 21]. This T-stub offers better impedance matching and improves MC. The  $S$ -parameters with and without T-stub for the T-

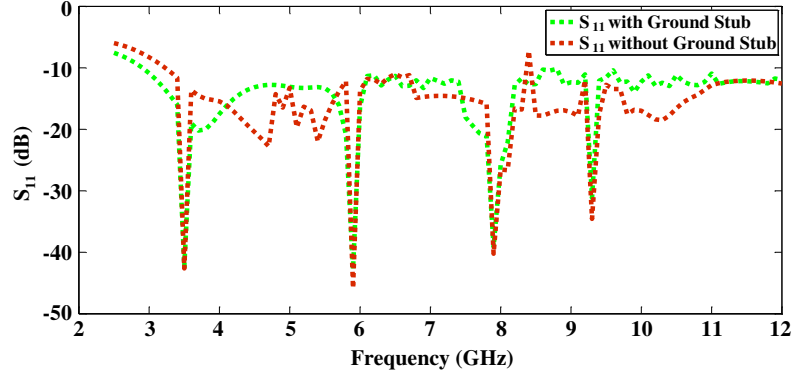


**Figure 5.**  $S_{11}$  of the proposed MIMO design with and without T-Stub and ground slot.

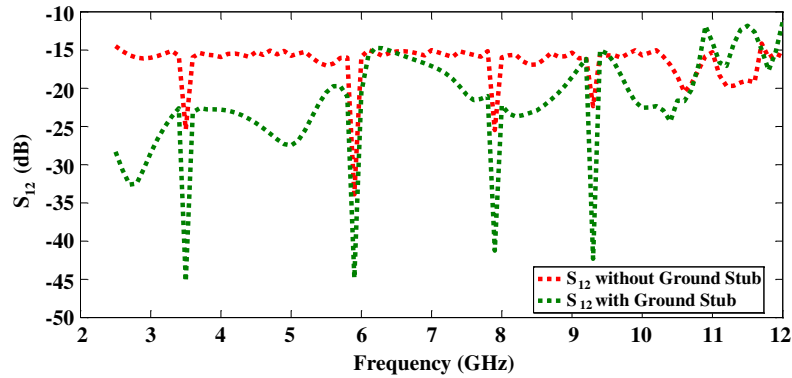


**Figure 6.**  $S_{12}$  of the proposed MIMO antenna with and without T-stub and ground slot.

slotted MIMO design are compared in Figures 5 and 6. From Figure 5, using a T-stub and making the antenna structure as a T-slotted antenna, resonant peaks are shifted from 4.0 to 3.5 GHz, 7.5 to 7.9 GHz, and 10 to 9.3 GHz. This shift is due to the T-stub that acts as a reflector.  $S_{12} > -15$  dB over the entire UWB range with specific applications at WiMAX (3.5 GHz), WLAN (5.9 GHz), X-band SATCOM applications (7.9 GHz) and Radar, Mobile phones, and commercial WLAN (9.3 GHz).

### 3.2. Effect of the Ground Slot

Figure 5 and Figure 6 show  $S$ -parameter analysis for the T-shaped slotted MIMO antenna with and without slot on the ground. A small portion of the ground is cut as a slot to enhance isolation. It is observed in the  $S_{11}$  plot, and resonant peaks are shifted from 4.0 to 3.5 GHz, 7.5 to 7.9 GHz, and 10 to 9.3 GHz by using a ground slot.  $S_{21}$  is improved by removing or subtracting a slot in the ground. With the usage of the slot in the ground, the mutual coupling is reduced at WiMAX (3.5 GHz), WLAN (5.9 GHz), X-band SATCOM applications (7.9 GHz) and Radar, Mobile phones, and commercial WLAN (9.3 GHz) that makes  $S_{21} > -15$  dB.

### 3.3. Analysis of the Distribution of Surface Current for the Minimizing MC

Surface current distribution ( $J$ ) is analyzed for the minimization of MC among the MIMO elements. The ground stub effect and slot on current density ( $J$ ) at 3.5 GHz are analyzed in Figure 7. Figure 7 shows that port 1 is provided with strip-line feed and port 2 with  $50\ \Omega$  terminating impedance. It is identified that current reduction passes toward the stub on the ground and a slot, leading to surface current reduction minimizing the MC. Figure 7(b) illustrates the surface current when port one is ended with  $50\ \Omega$  impedance, and port 2 is excited. Similar to the first case, here also, there is a reduction in coupling current.

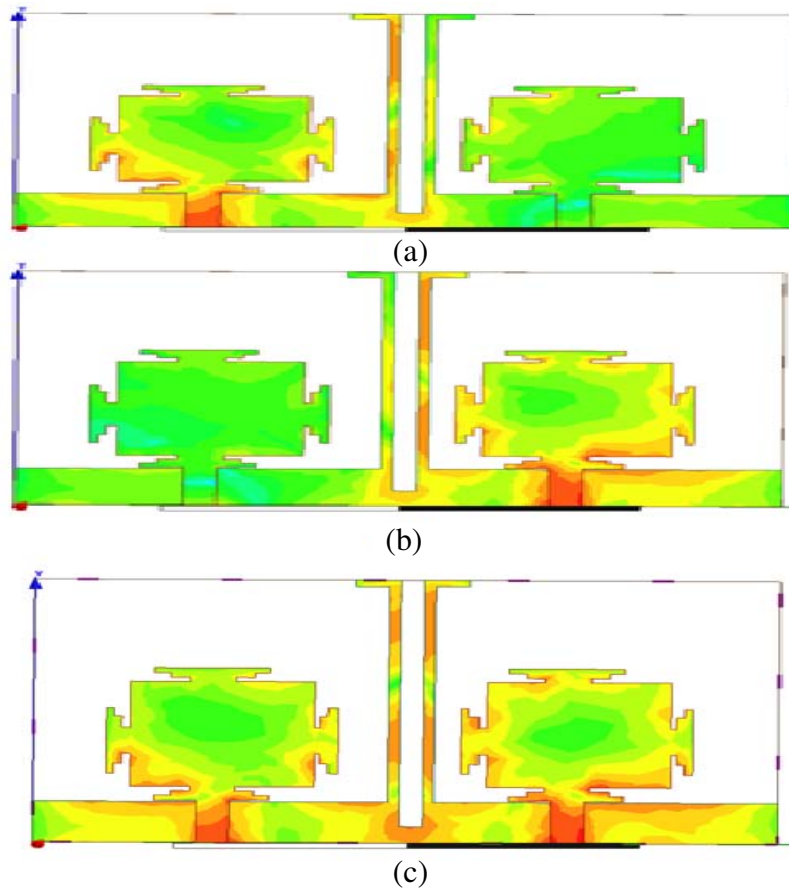


**Figure 7.** Distribution of the surface currents, (a) antenna when Port 1 is excited, (b) antenna when Port 2 is excited, (c) the proposed design when both the ports are excited.

#### 4. ANTENNA PARAMETRIC ANALYSIS

The response of the MIMO antenna on isolation improvement and the parametric analysis based on the distance between two patches are observed for  $|S_{11}|$  &  $|S_{12}|$  at  $d = 7$  mm,  $d = 8$  mm,  $d = 9$  mm,  $d = 9.5$  mm,  $d = 10$  mm, &  $d = 10.75$  mm with port 1 excited and port 2 with  $50\Omega$  terminating impedance. In this proposed method, one parameter is varied, and all the other parameters are static to analyze  $S$ -parameters with one of the two ports excited.

##### 4.1. Effect of Distance between Patch Elements

The distance variation between the patch elements will show an impact for various distances varying from  $d = 7$  mm to  $d = 10.75$  mm, and the analysis of the MIMO antenna is shown in Figures 8 & 9.

From Figure 8, at distance  $d = 10.75$  mm, resonating at 3.5 GHz, 5.9 GHz, 7.9 GHz, and 9.3 GHz,  $S_{11}$  is  $-42.62$  dB,  $-45.84$  dB,  $-40.23$  dB, and  $-34.56$  dB, and at these resonant frequencies with distance  $d = 10.75$  mm,  $S_{12}$  is  $-45.26$  dB,  $-44.83$  dB,  $-41.25$  dB, and  $-42.31$  dB and is plotted in Figure 9. When distance  $d = 10.75$  mm,  $S_{11}$  is  $> -40$  dB, and  $S_{12}$  is  $> -40$  dB which shows that there is a reduction of strong mutual coupling between two radiators.

When the patch distances are varied with  $d = 9$  mm, 9.5 mm, 10 mm,  $S_{11} > -20$  dB and  $S_{12} > -20$  dB. Distance variation from 7 mm to 10.75 mm using parameter analysis, optimized distance  $d = 10.75$  mm, reduces the MC at WiMAX (3.5 GHz), WLAN (5.9 GHz), X-band SATCOM applications (7.9 GHz) and Radar, Mobile phones, and commercial WLAN (9.3 GHz).

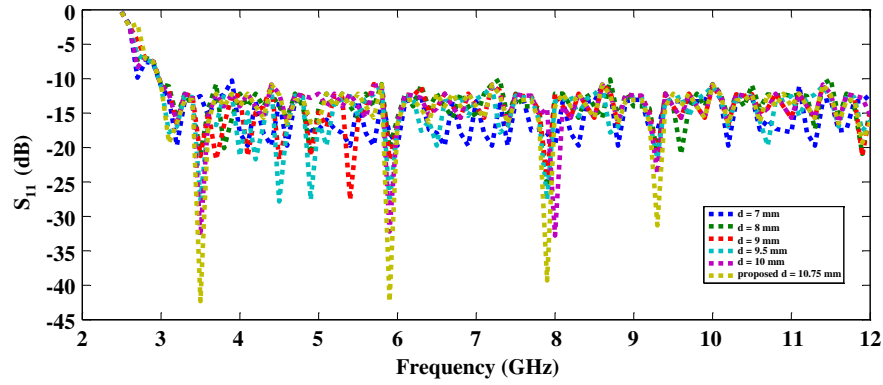


Figure 8.  $S_{11}$  for different distances of the proposed MIMO antenna.

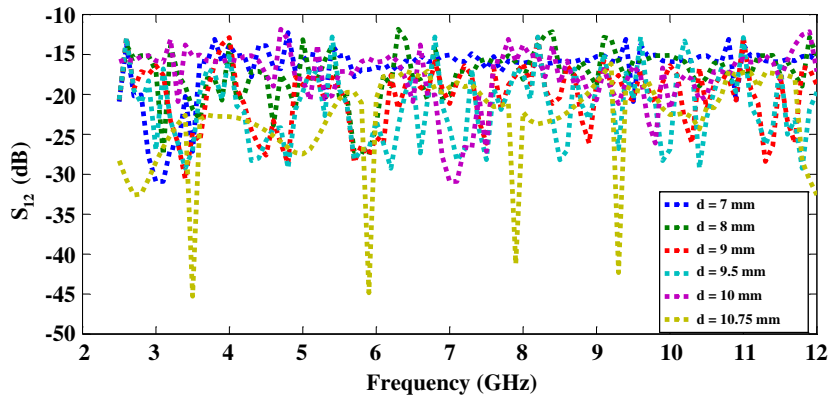


Figure 9.  $S_{12}$  for different distances of the proposed MIMO design.

#### 4.2. Varying Parameter Lengths $L_1$ , $L_2$ , and $L_3$ Effects

$L_1$ ,  $L_2$ , and  $L_3$  variations will affect the parameters like  $S_{11}$ ,  $S_{12}$ , directivity, and gain. From Figure 10, by varying  $L_1$ ,  $L_2$ , and  $L_3$ ,  $S_{11}$  increases by 15 dB for UWB frequencies suitable for WiMAX (3.5 GHz), WLAN (5.9 GHz), X-band SATCOM applications (7.9 GHz) and Radar, Mobile phones, and commercial WLAN (9.3 GHz).

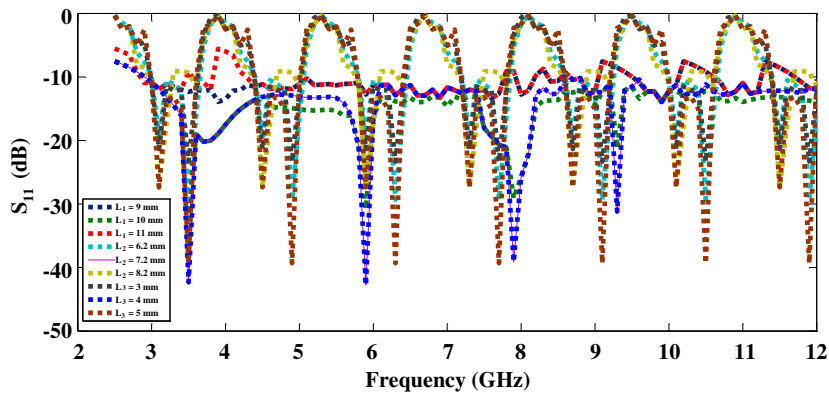
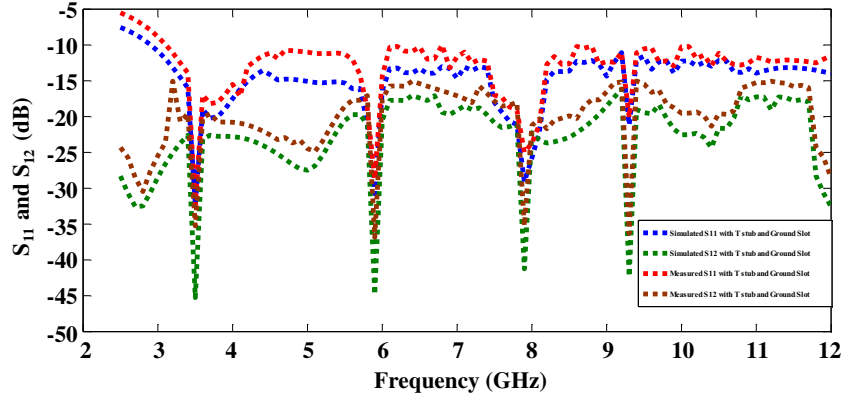


Figure 10.  $S_{11}$  for different lengths of the T-slotted MIMO design.

## 5. SIMULATION AND MEASUREMENT RESULTS

### 5.1. S-Parameters and Radiation Performance

For the validation of the proposed design, an antenna is fabricated, and measured results are obtained with Keysight (model N9916A) VNA. Simulated and measured results differ due to fabrication errors and SMA connectors. Figure 11 illustrates the simulated and measured  $S$ -parameters. The IBW of the design is 7.6 GHz, which ranges from 3.1 GHz to 10.7 GHz (fractional BW of 64.6%) with  $S_{21}$  below  $-39$  dB. The measured and simulated results are obtained by exciting one port and simultaneously with  $50\ \Omega$  for the other port. The 2-D radiation plot of the proposed design in  $E$ -plane and  $H$ -plane for the operating frequencies is illustrated in Figure 12.



**Figure 11.** Simulated and measured  $S_{11}$  and  $S_{12}$  for the T-slotted MIMO design.

Figure 12 shows radiation patterns for the simulated design at the resonant frequency. A 4.95 dBi measured gain is obtained for the fabricated design, and 5.80 dBi is the simulated realized peak gain, shown in Figure 13. Figures 14 and 16 illustrate the  $H$ -plane and  $E$ -plane co-polarization and cross-polarization patterns. Figure 15 illustrates the fabricated T-slotted MIMO antenna. A detailed comparison of different antenna designs with the proposed structure is indicated in Table 2.

### 5.2. Diversity Performance of the Proposed Design

The capacity of the proposed MIMO design is validated using the parameters ECC and DG. The parameter results and measured results are compared. ECC explains how accurately antenna-1 characteristic is associated with other antennas' characteristic when they are nearby. ECC analysis can be done using  $S$ -parameters as indicated [29]; the proposed design's ECC is  $< 0.05$ , and the plot is shown in Figure 17. Figure 18 shows the DG plot with 9.9 dB for operating frequency and indicates the proposed design's good diversity performance.

The ECC formula in terms of  $S_{12}$  is given below in terms of field-based equations in terms of  $\theta$  and  $\Phi$  which is written in Equation (8) and indicates the radiation patterns of two different antennas' correlation.

$$\rho_e = \frac{\left| \int_0^{2\pi} \int_0^\pi (XPR \cdot E_{\theta 1} \cdot E_{\theta 2}^* \cdot P_\theta + E_{\varphi 1} \cdot E_{\varphi 2}^* \cdot P_\varphi) d\Omega \right|^2}{\int_0^{2\pi} \int_0^\pi (XPR \cdot E_{\theta 1} \cdot E_{\theta 2}^* \cdot P_\theta + E_{\varphi 1} \cdot E_{\varphi 2}^* \cdot P_\varphi) d\Omega \times \int_0^{2\pi} \int_0^\pi (XPR \cdot E_{\theta 1} \cdot E_{\theta 2}^* \cdot P_\theta + E_{\varphi 1} \cdot E_{\varphi 2}^* \cdot P_\varphi) d\Omega} \quad (8)$$

DG is the decreased required receiving SNR for a given BER averaged over the fading. Explicitly, this is the reduction in a fading margin obtained by minimizing the fading with the MIMO antenna.

$$DG = 10\sqrt{1 - \text{ECC}} \quad (9)$$

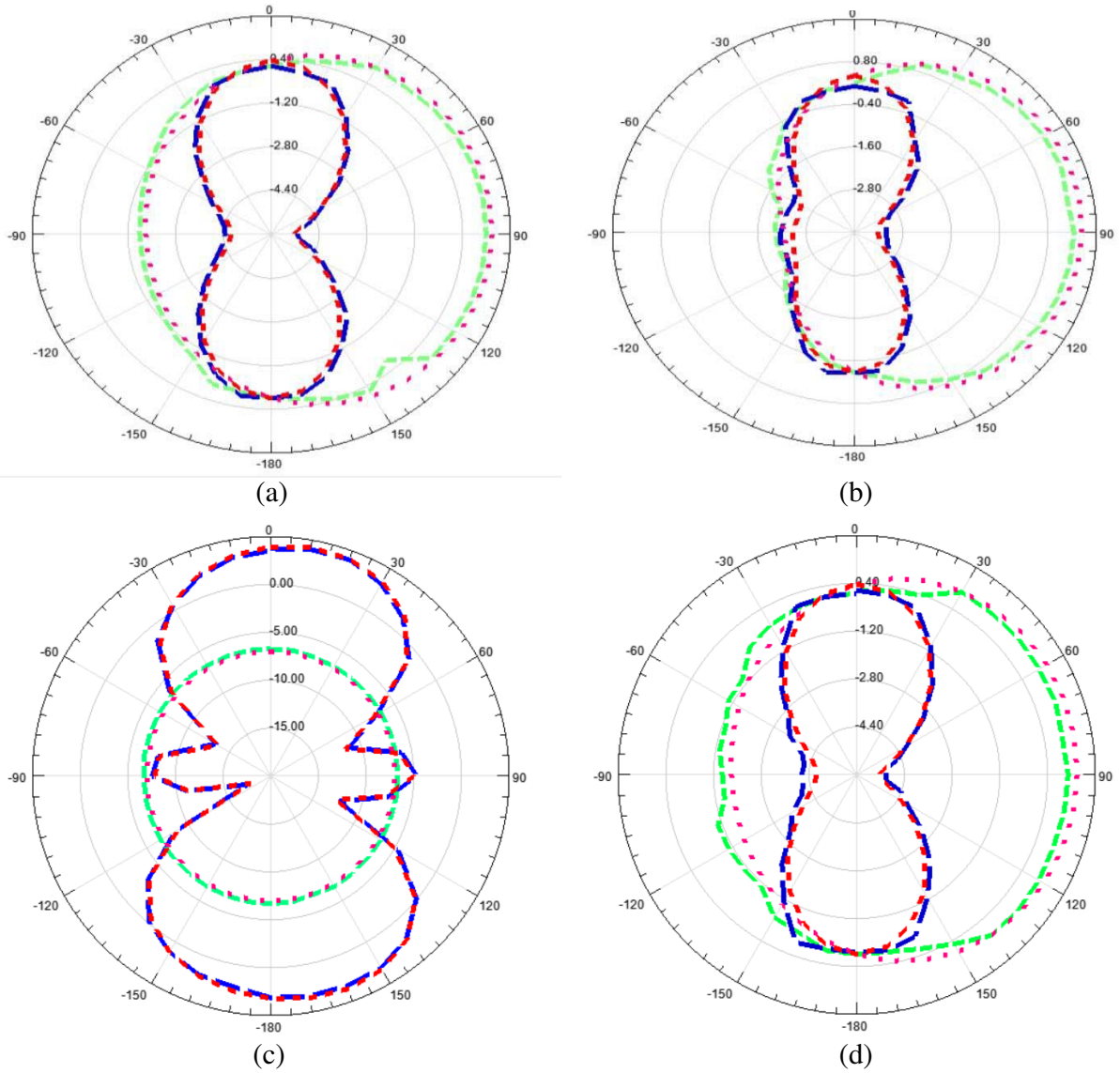


**Figure 12.** 2-D radiation patterns at (a) 3.5 GHz, (b) 5.9 GHz, (c) 7.9 GHz, (d) 9.3 GHz in *E*-Plane and *H*-Plane of the proposed MIMO antenna (red color: simulated in *E*-Plane, blue color: measured in *E*-Plane, pink color: simulated in *H*-Plane, green color: measured in *H*-Plane).

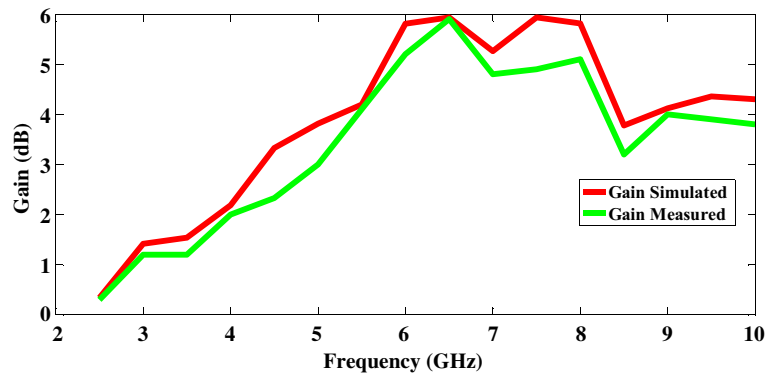


**Figure 13.** Gain of the proposed MIMO design.

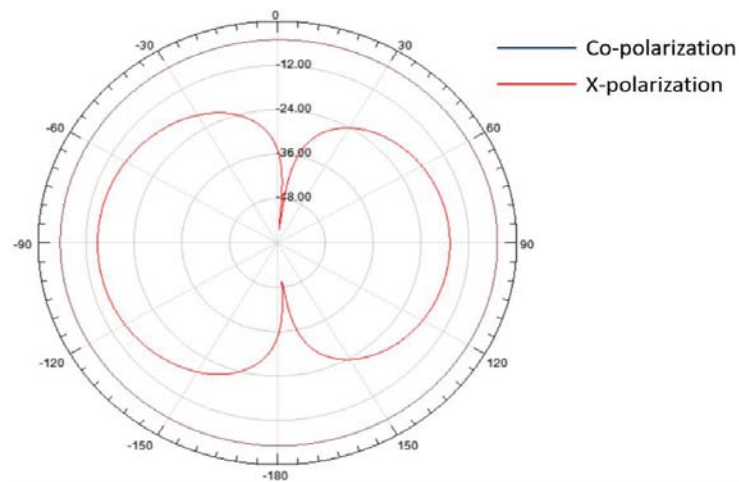


Figure 14. Co- and cross-polarization in  $H$ -plane at 3.5 GHz.

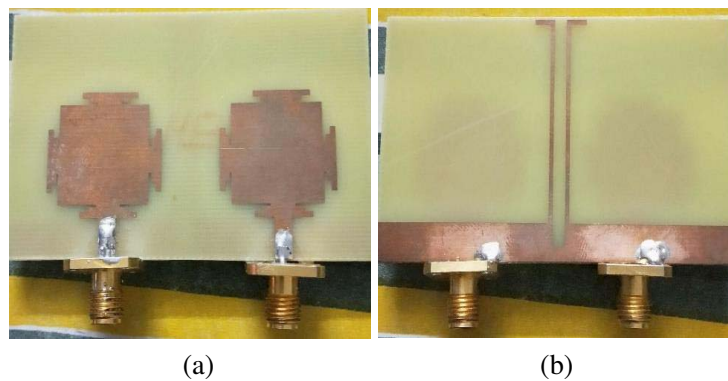


Figure 15. Fabricated model, (a) front view, (b) back view.

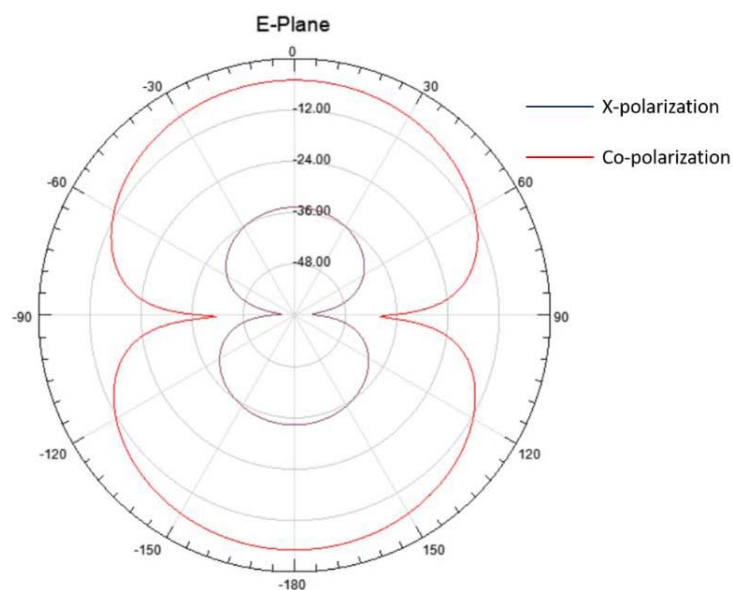


Figure 16. Co- and cross-polarization in  $E$ -plane at 3.5 GHz.

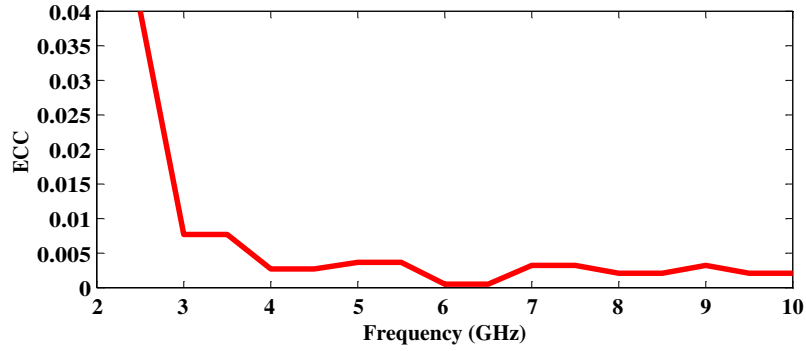


Figure 17. Simulated ECC of the proposed design.

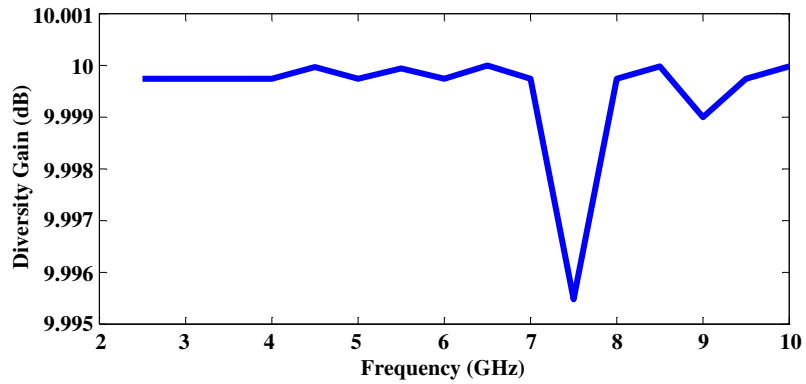
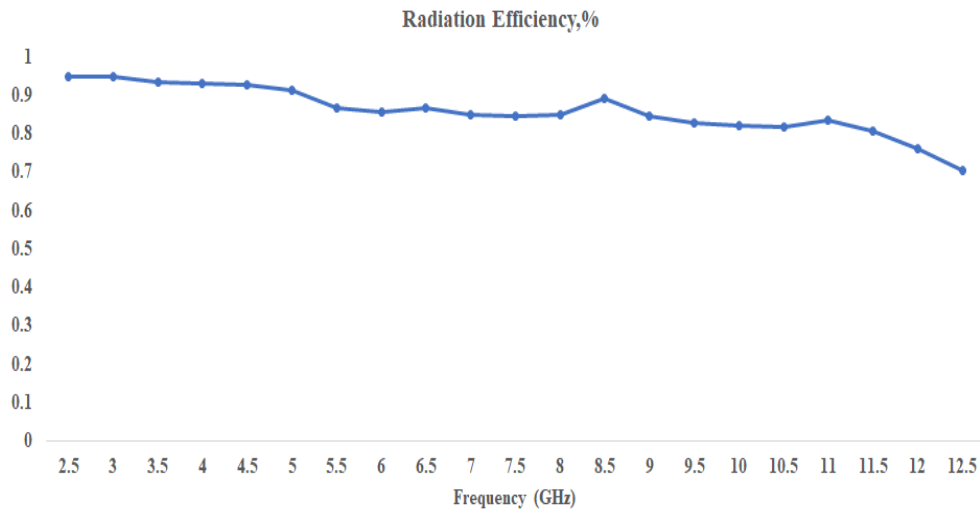


Figure 18. Diversity gain of the proposed MIMO antenna.

Table 2. Comparison of the present work and those of previously reported works.

Reference	Antenna Dimensions (mm)	$S_{11}$ (dB)	$S_{12}$ (dB)	Frequency (GHz)	Substrate used
[2]	$30 \times 55 \times 1.524$	-22	-20	3.5	Rogers RO4350B
[5]	$20.5 \times 30.1 \times 0.787$	-20	-25	3.1–10.6	RT/Duroid 5880
[7]	$20 \times 24 \times 1.6$	-32	-34	7.8 and 14.2	FR-4 Epoxy
[8]	$24 \times 32 \times 0.8$	$> -10$	$> -15$	3.1–12.5	FR-4 Epoxy
[13]	$36 \times 30 \times 1.56$	-25	-42	5.8	RT/Duroid 5880
[14]	$20 \times 46 \times 1.6$	-40	-22	5.8	FR-4 Epoxy
[19]	$55 \times 28 \times 1.6$	-25	-49	3.46–3.69	FR-4 Epoxy
Proposed method	$50 \times 25 \times 1.6$	$> -10$ with four resonant peaks at 3.5, 5.9, 7.9, and 9.3 GHz	$> -15$ with four resonant peaks at 3.5, 5.9, 7.9, and 9.3 GHz	3.1–10.6	FR-4 Epoxy



**Figure 19.** Radiation efficiency (%) of the proposed MIMO antenna.

DG depends on BER and has a maximum limit of the fading margin, irrespective of the number of antennas used. The radiation efficiency is plotted in Figure 19. From the figure, the radiation efficiency is greater than 95%. The total efficiency of the MIMO antenna is calculated using the formula [30].

$$\text{Total Efficiency} = (1 - |\text{TARC}|^2) * \text{Radiation efficiency} \quad (10)$$

## 6. CONCLUSION

A T-slotted antenna with a size of  $65 \times 40 \text{ mm}^2$  is investigated. Two T-slotted monopole elements operate for WiMAX and WLAN applications in the range of 2.77 GHz–6.55 GHz with an impedance bandwidth of 64.6%. To validate the design, a MIMO antenna with two elements is fabricated and tested. The edge-to-edge spacing between the two radiators is only  $0.215\lambda_0$ . A T-stub with a slot improves isolation at the operating resonant frequencies 3.5 GHz, 5.9 GHz, 7.9 GHz, and 9.3 GHz with  $S_{12} > -15 \text{ dB}$ . Mutual coupling is significantly reduced by etching a T-shape stub using a slot on the ground. The realized peak gain is 4.95 dBi for the fabricated antenna. Diversity gain (DG) is about 9.9 dB and ECC  $< 0.05$ , respectively, over the UWB range.

## ACKNOWLEDGMENT

I convey my sincere thanks to Dr. M. V. S. Prasad, Professor, R V R & J C College of Engineering, Guntur, Andhra Pradesh, India, for providing necessary guidance, and thanks for the R&D wing, ANU College of Engineering and Technology, Guntur, Andhra Pradesh, India for proper suggestions, and K. Prem Chand, Assistant Professor, for fabrication and testing antenna results as a part of research work.

## REFERENCES

1. Biswas, A. K. and U. Chakraborty, "Reduced mutual coupling of compact MIMO antenna designed for WLAN and WiMAX applications," *Int. J. RF Microw. Comput. Aided Eng.*, e21629, 2018.
2. Abdullah, M., Q. Li, W. Xue, G. Peng, Y. He, and X. Chen, "Isolation enhancement of MIMO antennas using shorting pins," *Journal of Electromagnetic Waves and Applications*, Vol. 33, No. 10, 1249–1263, 2019.
3. Babu, K. V. and B. Anuradha, "Design of inverted L-shape & ohm symbol inserted MIMO antenna to reduce the mutual coupling," *Int. J. Electron. Commun. (AEÜ)*, Vol. 105, 42–53, 2019.

4. Xi, L., H. Zhai, and L. Li, "A low-profile antenna system with a compact new structure for reducing mutual coupling," *Journal of Electromagnetic Waves and Applications*, Vol. 33, No. 1, 71–83, 2018.
5. Babashah, H., H. R. Hassani, and S. Mohammad-Ali-Nezhad, "A compact UWB printed monopole MIMO antenna with mutual coupling reduction," *Progress In Electromagnetics Research C*, Vol. 91, 55–67, 2019.
6. Liu, Y., X. Yang, Y. Jia, and Y. Jay Guo, "A low correlation and mutual coupling MIMO antenna," *IEEE Access*, Vol. 7, 127384–127392, 2019, doi: 10.1109/ACCESS.2019.2939270.
7. El Ouahabi, M., A. Zakriti, M. Essaaidi, A. Dkiouak, and E. Hanae, "A miniaturized dual-band MIMO antenna with low mutual coupling for wireless applications," *Progress In Electromagnetics Research C*, Vol. 93, 93–101, 2019.
8. Gurjar, R., D. K. Upadhyay, B. K. Kanaujia, and K. Sharma, "A novel compact self-similar fractal UWB MIMO antenna," *Int. J. RF Microw. Comput. Aided Eng.*, e21632, 2018.
9. Nadeem, I. and D.-Y. Choi, "Study on mutual coupling reduction technique for MIMO antennas," *IEEE Access*, Vol. 7, 2019, doi: 10.1109/ACCESS.2018.2885558.
10. Salehi, M. and A. Tavakoli, "A novel low mutual coupling microstrip antenna array design using the defected ground structure," *Int. J. Electron. Commun. (AEÜ)*, 718–723, 2006, doi:10.1016/j.aeue.2005.12.009.
11. Anitha, R., V. P. Sarin, P. Mohanan, and K. Vasudevan, "Enhanced isolation with defected ground structure in MIMO antenna," *Electronics Letters*, Vol. 50, No. 24, 1784–1786, November 20, 2014.
12. Luo, C.-M., J.-S. Hong, and L.-L. Zhong, "Isolation enhancement of a very compact UWB-MIMO slot antenna with two defected ground structures," *IEEE Antennas and Wireless Propagation Letters*, Vol. 14, 1766–1769, 2015.
13. Sun, X.-B. and M. Y. Cao, "Low mutual coupling antenna array for WLAN application," *Electronics Letters*, Vol. 53, No. 6, 368–370, March 16, 2017.
14. Kumar, N. and U. K. Kommuri, "MIMO antenna  $H$ -plane isolation enhancement using UC-EBG structure and metal line strip for WLAN applications," *Radio Engineering*, Vol. 29, No. 2, 399–406, June 2019, doi: 10.13164/re.2019.0399.
15. Xiao, S., M.-C. Tang, Y.-Y. Bai, S. Gao, and B.-Z. Wang, "Mutual coupling suppression in microstrip array using defected ground structure," *IET Microw. Antennas Propag.*, Vol. 5, No. 12, 1488–1494, 2011, doi: 10.1049/iet-map.2010.0154.
16. Ghaloua, A., J. Zbitou, L. El Abdellaoui, M. Latrach, A. Tajmouati, and A. Errkik, "Reduction of mutual coupling between closely spaced microstrip antennas arrays using electromagnetic band-gap (2D-EBG) structures," *TELKOMNIKA*, Vol. 16, No. 1, 151–158, February 2018, ISSN: 1693-6930, doi: 10.12928/TELKOMNIKA.v16i1.7017.
17. Thakur, E., N. Jaglan, S. D. Gupta, and B. K. Kanaujia, "A compact notched UWB MIMO antenna with enhanced performance," *Progress In Electromagnetics Research C*, Vol. 91, 39–53, 2019.
18. Dwairi, M. O., M. S. Soliman, A. A. Alahmadi, S. H. A. Almalki, and I. I. M. Abu Sulayman, "Design and performance analysis of fractal regular slotted-patch antennas for ultra-wideband communication systems," *Wireless Personal Communications*, Vol. 105, 819–833, February 5, 2019, doi: 10.1007/s11277-019-06123-5.
19. Biswas, A. K., A. Kundu, A. K. Bhattacharjee, and U. Chakraborty, "Isolator-based mutual coupling reduction of H-shaped patches in MIMO antenna applications," *Advances in Computer, Communication and Control, Lecture Notes in Networks and Systems*, Vol. 41, 361–366, 2019, doi:10.1007/978-981-13-3122-0\_34.
20. Ghosh, J., D. Mitra, and S. Das, "Mutual coupling reduction of slot antenna array by controlling surface wave propagation," *IEEE Transactions on Antennas and Propagation*, Vol. 67, No. 2, 1352–1357, February 2019.
21. Liu, L., S. W. Cheung, and T. I. Yuk, "Compact MIMO antenna for portable UWB applications with band-notched characteristic," *IEEE Transactions on Antennas and Propagation*, Vol. 63, No. 5, 1917–1924, 2015.

22. Choukiker, Y. K., S. K. Sharma, and S. K. Behera, "Hybrid fractal shape planar monopole antenna covering multiband wireless communications with MIMO implementation for handheld mobile devices," *IEEE Transactions on Antennas and Propagation*, Vol. 62, No. 3, 1483–1488, March 2014.
23. Lalbakhsh, A., A. A. Lotfi Neyestanak, and M. Naser-Moghaddasi, "Microstrip hairpin bandpass filter using modified minkowski fractal-shape for suppression of second harmonic," *IEICE Trans. Electron.*, Vol. E95-C, No. 3, 378–381, March 2012.
24. Lalbakhsh, A., M. U. Afzal, K. P. Esselle, and S. L. Smith, "Low-cost nonuniform metallic lattice for rectifying aperture near-field of electromagnetic bandgap resonator antennas," *IEEE Transactions on Antennas and Propagation*, Vol. 68, No. 5, 3328–3335, May 2020.
25. Lalbakhsh, A., M. U. Afzal, K. P. Esselle, S. L. Smith, and B. A. Zeb, "Single-dielectric wideband partially reflecting surface with variable reflection components for realization of a compact high-gain resonant cavity antenna," *IEEE Transactions on Antennas and Propagation*, Vol. 67, No. 3, 1916–1921, March 2019.
26. Lalbakhsh, A., M. U. Afzal, K. P. Esselle, and S. L. Smith, "A high-gain wideband EBG resonator antenna for 60 GHz unlicensed frequency band," *12th European Conference on Antennas and Propagation (EuCAP 2018)*, 2018.
27. Papadopoulos, K. A., C. A. Papagianni, P. K. Gkonis, I. S. Venieris, and D. I. Kaklamani, "Particle swarm optimization of antenna arrays with efficiency constraints," *Progress In Electromagnetics Research M*, Vol. 17, 237–251, 2011.
28. Lalbakhsh, A., M. U. Afzal, and K. P. Esselle, "Multi-objective particle swarm optimization to design a time delay equalizer metasurface for an electromagnetic band gap resonator antenna," *IEEE Antennas and Wireless Propagation Letters*, Vol. 16, 912–915, 2016.
29. Jamshidi, M., A. Lalbakhsh, B. Mohamadzade, H. Siahkamari, and S. M. H. Mousavi, "A novel neural-based approach for design of microstrip filters," *Int. J. Electron. Commun. (AEÜ)*, Vol. 110, 152847, 2019.
30. Wang, M., T.-H. Loh, Y. Zhao, and Q. Xu, "A closed-form formula of radiation and total efficiency for lossy multiport antennas," *IEEE Antennas and Wireless Propagation Letters*, Vol. 18, No. 12, 2468–2472, 2019.